Kovove Mater. 54 2016 407–416
DOI: 10.4149/km_2016_6_407

Microstructure of fibre laser welded joint of dual phase steel with bake hardening steel

P. Švec[1]*, A. Schrek[1], M. Dománková[2]

[1]*Institute of Technologies and Materials, Faculty of Mechanical Engineering, Slovak University of Technology in Bratislava, Pionierska 15, 831 02 Bratislava, Slovak Republic*
[2]*Institute of Materials Science, Faculty of Materials Science and Technology in Trnava, Slovak University of Technology in Bratislava, Bottova 25, 917 24 Trnava, Slovak Republic*

Received 15 July 2016, received in revised form 3 August 2016, accepted 4 August 2016

Abstract

The fibre laser welding of dual phase DP600 steel and bake hardening BH220 steel were studied with a concentration on the microstructure of butt joints, but microhardness and tensile properties were also measured. The temperature peaks influenced the microstructure of the fusion zone and heat affected zone. The microstructure in the fusion zone was predominantly built of acicular ferrite with small areas of upper and lower bainite, and martensite. The similar microstructure was observed in the heat affected zone near DP600 steel. The microstructure in the heat affected zone near BH220 steel consisted mostly of coarse ferrite and acicular ferrite. The microhardness increased in the fusion zone and in the heat affected zone near DP600 steel, which was the consequence of martensite and bainite formation in these areas. The tensile strength of the fibre laser welded joints exceeded the strength of the BH220 steel base material with failure occurring in this steel.

K e y w o r d s: dual phase steel, bake hardening steel, fibre laser welding, microstructure, microhardness

1. Introduction

Recently dual phase (DP) steels have found widespread application as structural components due to their excellent properties. Some of the major advantages of the DP steels include their superior mechanical properties in comparison with standard steels, moderate price thanks to the small amount of alloying additions, as well as excellent technological properties, together with good weldability and formability [1–5]. They can be used in the manufacture of lightweight automobiles to reduce fuel consumption without compromising other attributes such as safety, performance, recyclability, and cost. Frames, crossbeams, vertical beams, side impact beams, and safety elements are often made of DP steels [6–8]. The excellent mechanical properties of DP steels are the consequence of their multiphase structure. The microstructure of DP steel usually consists of 10–30 % martensite in the fine-grained, spherical ferrite matrix, but there are DP steels even with the portion above 50 % of martensite. As a result, the steels are characterized by high tensile strength up to 1200 MPa with unit elongation up to 27 % [9, 10]. Most often the microstructure of DP steel is developed as a result of accelerated cooling of thin sheets after cold rolling in the range between A_{c1} and A_{c3} and controlled air-water mist cooling to ambient temperature. The process is a flexible one and allows different combinations of the relative volume ratio of ferrite and martensite [2, 11, 12]. Bake hardening (BH) steels are an important part of high strength low alloy steels (HSLA). Although they are still predominantly used in structural applications, their application in auto industry is rapidly increasing. Due to the low carbon and alloying element content, BH steels have mainly ferritic microstructure. This microstructure is the consequence of lower strength, but better formability and weldability compared to DP steels [4, 13–15].

When joining DP steels with BH steels in tailor

*Corresponding author: tel.: +421 905326211; e-mail address: pavol.svec@stuba.sk

Table 1. Maximal concentration, c_{max} (wt.%), of alloying elements in dual phase steels DP600

Element	C	Mn	Si	Al	P	S	V	B	Cr + Mo	Nb + Ti
c_{max}	0.17	2.2	0.8	2.0	0.08	0.015	0.2	0.05	1	0.15

Table 2. Maximal concentration, c_{max} (wt.%), of alloying elements in bake hardening steel BH220

Element	C	Mn	Si	Al	P	S	Nb	Ti
c_{max}	0.1	0.07	0.5	0.1	0.08	0.025	0.09	0.12

welded blank (TWB) parts, the good ratio of strength--deformation properties can be achieved. The DP steel assigns the strength of the part and BH steel assigns the deformation zone because of its ferritic structure and excellent formability. The TWBs are semi--finished parts that consist of at least two single sheets that are welded together prior to the forming process. The sheets can exhibit different mechanical properties, thickness or coatings. Using TWBs enables an adaptation to locally different loading conditions or other requirements in the part [16, 17]. Other advantages of joining prior to the forming are the reduction of the number of the required forming tools, the higher accuracy in the forming process and the enhanced use of material which leads to lower production costs. The most important advantage of a part made from TWBs is the weight reduction compared to conventional products. A car body manufactured using TWBs and high strength steels can achieve a 25 % weight reduction [3, 18, 19].

In series production, the joining of TWBs is usually done by laser welding though other weld techniques are also possible. Among commercial laser systems, fibre lasers have the characteristics of excellent beam quality and high brightness, and consequently, they have attracted more attention over the last decade for cutting, welding, and cladding applications [1, 20]. Low heat input is an important characteristic of laser welding, and it is the consequence of small fusion zone (FZ) and heat-affected zone (HAZ) and the lower cost and greater flexibility compared to other welding methods. Low heat input welding methods can produce the fine grain structures that provide the strength and toughness of the joint, and they also have the benefit of decreasing welding thermal distortion [1, 21, 22].

Microstructure changes accompanying the laser welding increase the strength in weld region of TWB but also worsen its formability. The proper microstructure assures proper ratio between strength and formability [3, 4, 23]. The microstructure is affected mainly by the chemical composition of base materials, sheets thicknesses and welding parameters such as power input, welding speed and others. The final microstructure in FZ and HAZ weld is a consequence of rapid heating and cooling cycles with melting and solidification happening in a significantly short time. FZ and HAZ are characterized by increased hardness and decreased plastic properties. The welding process influences the weld imperfections, which are related to the weld geometry such as concavity, sagging, impurities or gaseous elements, porosity, pinholes or craters [13, 14, 24]. Several works were devoted to the laser welding of different DP steels, but fewer works were focused on welding of DP steels with BH steels. Many papers which presented laser welding of DP steels were concentrated on microstructure and hardness of welded joints. Some authors studied the effect of hardness increase in the FZ and HAZ in DP steels after laser welding process on the properties of joints. The higher hardness causes reduction of formability and even significant lack of toughness [3, 4, 13–15]. Several authors described the reduction of hardness in the tempered region of HAZ; a phenomenon is generally known as HAZ softening. HAZ softening has detrimental effects on the weld properties with strain localization in the HAZ at lower stress than may be supported by the base material (BM) [7, 23, 25–27]. Since more information about microstructure evolution of fibre laser welded joints is needed, this work attempts to characterize the microstructure of DP600 and BH220 steel fibre laser welded joints and its correlation with microhardness profile across the welded joints.

2. Experimental procedures

Two different steel sheets: dual phase DP600 steel and bake hardening BH220 steel with a thickness of 1.2 mm and zinc coating of 100 g m^{-2} were used for fibre laser welding. The chemical composition of the experimental steels is given in Tables 1 and 2 and their mechanical properties are compared in Table 3. Used steels differ in contents of alloying elements. The DP600 grade dual phase steel has a higher amount of these elements which is the consequence of higher strength and lower plasticity compared to BH220 grade bake hardening steel (Table 3). The max-

Table 3. Mechanical properties of experimental steels

Steel	Tensile strength (MPa)	Proof strength (MPa)	Elongation (%)
DP600	min. 600	340–420	min. 20
BH220	320–400	220–280	min. 32

imal concentration of Al (2.0 %) given in standards for DP600 steel is quite high, but the typical concentration is about 0.04 % Al.

The welding experiments were done on the solid-state fibre laser IPG type YLR 4500 with a maximum output of 4.5 kW, the wavelength of 1060 nm and a fibre diameter of 100 μm. Welding experiments were conducted on sheets with the length of 200 mm and width of 100 mm along the longitudinal edge. Prior to welding abutting surfaces were cleaned with steel wire brush followed by acetone swabbing. The butt joints were prepared at different welding parameters, but for this study welded joints prepared at a beam power of 1500 W and a welding speed of 30 mm s^{-1} were chosen. The distance of welding head was 250 mm, the focal position was 10 mm, and samples were prepared without filler metal and without shielding atmosphere.

The macrostructures of the laser weld surfaces were observed on the stereomicroscope Zeiss. The microstructure was studied on samples cut off the welding joints and prepared using standard metallographic techniques. The microstructures were observed using Axiovert 40MAT light microscope, JEOL JSM-IT300 scanning electron microscope (SEM) and two transmission electron microscopes (TEM) JEOL 200 CX with an accelerating voltage of 200 kV and Philips CM 300 with an accelerating voltage of 300 kV. Both carbon replica samples and thin film samples were prepared for TEM analysis. Selected area electron diffraction was used for qualitative phase analysis of weld sub-zones. Energy-dispersive spectroscopy (EDS) was employed for chemical analysis of particular phases. Image analysis was used to measure grain sizes of base materials. Microhardness surveys were performed on transverse sections of weld bead centres parallel to the surfaces of sheets using Vickers indenter with a load of 100 g. The samples for tensile tests were prepared from welded joints and tests were carried out using universal testing machine Instron 195 at room temperature and a crosshead speed of 50 mm min^{-1}.

3. Results

3.1. Microstructures of base materials

The SEM micrograph revealing microstructure of DP600 steel, which consists of the martensitic island in ferrite matrix steel, is documented in Fig. 1.

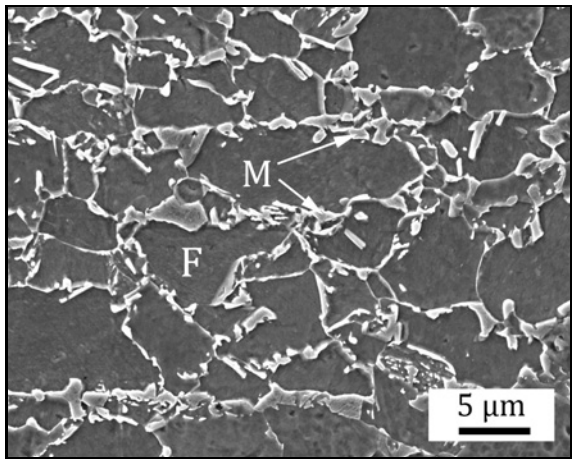

Fig. 1. The microstructure of the DP600 steel, SEM (M – martensite, F – ferrite).

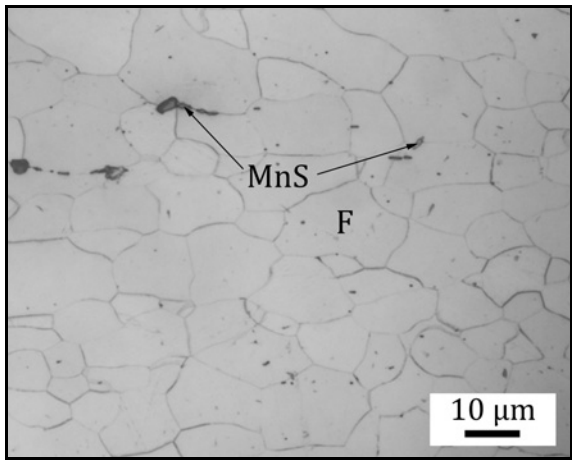

Fig. 2. The microstructure of BH220 steel, LM (F – ferrite, MnS – manganese sulphide inclusions).

The microstructure of DP600 steel is fine grained with equiaxed character, but it shows slight crystallographic texture which is built by equiaxed ferritic grains with an average size of 7 ± 1.5 μm and rows of martensite including a small portion of tempered martensite. The presence of tempered martensite can be explained by high martensite start temperature (Ms) of DP600 steel about 441 ℃ and so the martensite can self-temper immediately after transformation

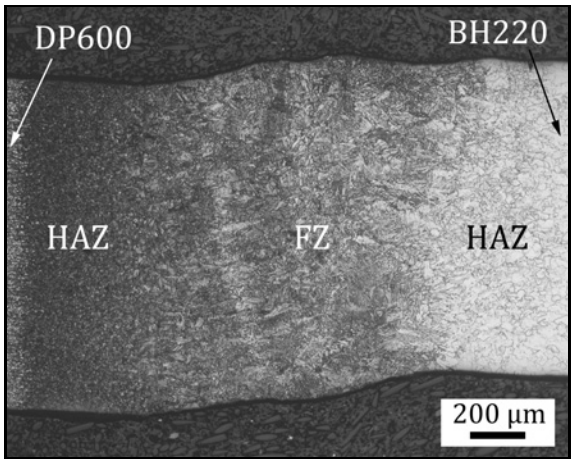

Fig. 3. The macrostructure of welded joint of DP600 steel with BH220 steel, LM (FZ – fusion zone, HAZ – heat affected zone).

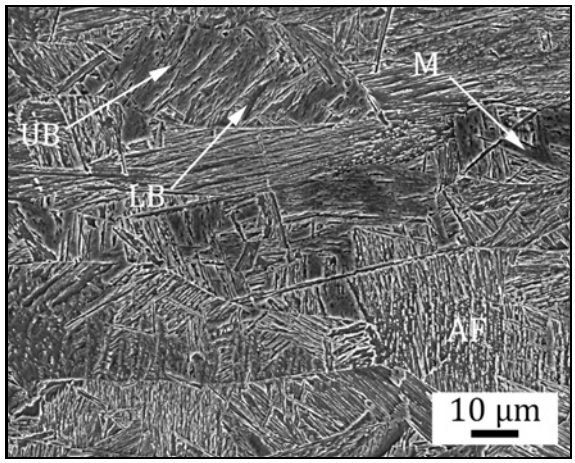

Fig. 4. Microstructure in FZ of the weld, SEM (AF – acicular ferrite, UB – upper bainite, LB – lower bainite, M – martensite).

[21, 28]. According to the work [28] the DP steel consists of 75 % martensite, 24 % ferrite and 1 % retained austenite. The microstructure of BH220 steel in Fig. 2 has a ferritic microstructure with relative homogeneous grain size, and with the average grain size of 10 ± 3 µm. There are some inclusions visible in Fig. 2. These were identified by EDS analysis as MnS sulphides.

3.2. Macrostructure of fibre laser welded joint

The macrostructure of a cross section of welded joint can be seen in Fig. 3. Particular sub-zones of the weld can be distinguished. The FZ in the centre has a thickness approximately from 0.7 to 1.0 mm. The DP600 steel BM is on the left and the BH220 steel BM is on the right of Fig. 3. The HAZ near DP600 steel with a thickness from 0.7 to 0.9 mm is between the FZ and DP600 steel and the HAZ near BH220 steel with a thickness from 0.5 to 0.7 mm is between the FZ and BH220 steel. The sub-zones are characterized by quite narrow shapes which are typical for keyhole welding. There is no evidence of defects such as porosity, cracks, but the joint is characterized with the slight concavity of the face and root sagging. The grain size within both HAZs varies accordingly different peak temperatures reached during the welding thermal cycle which are the most important factors in determining the microstructural evolution. The grain size in both HAZs decreases with the distance from the weld boundaries with the largest grains (coarse-grained region) observed in the vicinity of the FZ with the highest peak temperature above A_{c3} temperature but under the solidus temperature.

3.3. Microstructure of fibre laser welded joint

Typical microstructure in FZ of the weld is in Fig. 4. The FZ consists of coarse columnar dendritic grains, which are oriented perpendicular to the fusion boundary because the rate of heat removing is maximal in the direction perpendicular to the fusion boundary and the grains tend to grow in that direction. A mixture of large areas of acicular ferrite (AF) and small areas of upper bainite (UB), lower bainite (LB), and martensite (M) was identified within a large columnar grain structure. The characteristics of these microstructures were observed at higher magnification using SEM and TEM microscopy and are presented in Figs. 5 to 13.

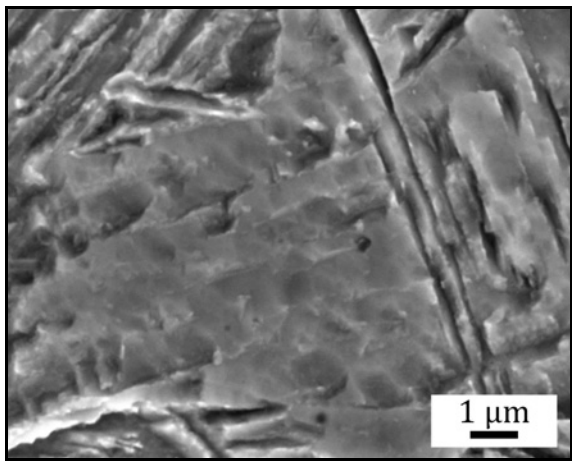

Fig. 5. Acicular ferrite in FZ of the weld, SEM.

The presence of acicular ferrite was dominant in the FZ and is in details documented in SEM micrograph in Fig. 5 and in two TEM micrographs in Fig. 6. Acicular ferrite in Fig. 5 is characterized by coarse ferritic laths. Figures 6a and 6b represent the bright and dark images of acicular ferrite, respectively. The

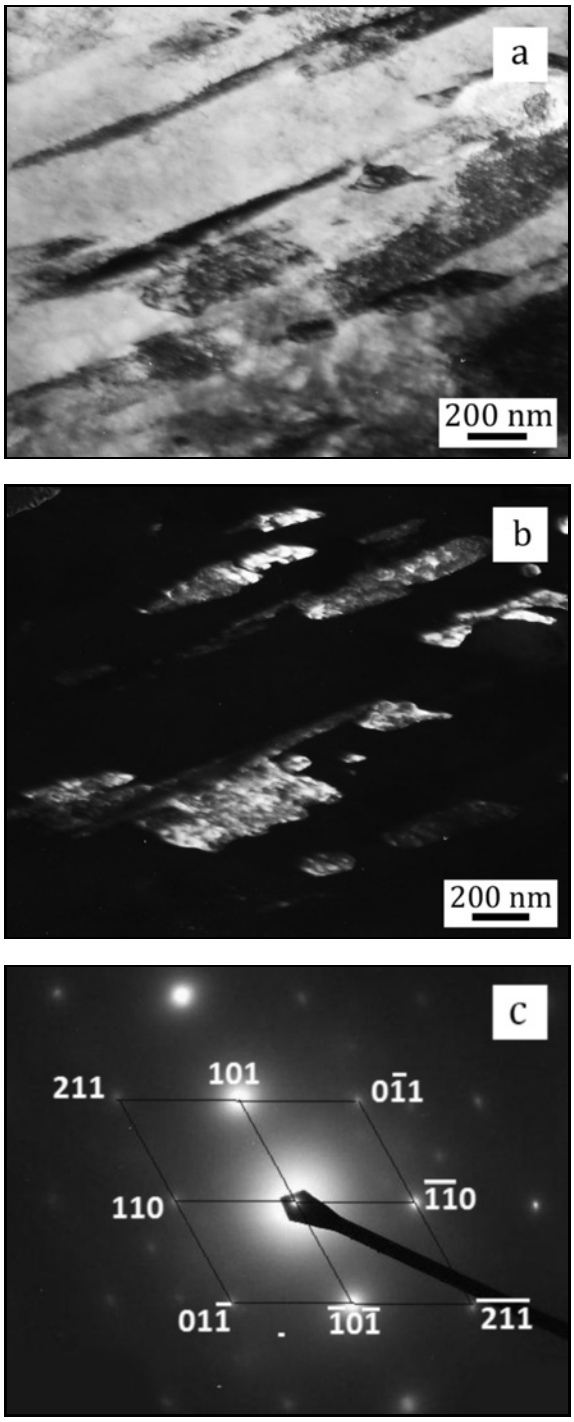

Fig. 6. Acicular ferrite in FZ of the weld: a) bright field TEM image, b) dark field TEM image with reflection of ferrite, c) electron diffraction pattern of BCC crystal structure of ferrite.

high density of dislocations can be seen inside the ferritic lath in bright field image in Fig. 6a. White areas in dark field image in Fig. 6b with reflections corresponding to the ferrite confirm the presence of ferrite. The electron pattern image in Fig. 6c verifies the BCC crystal structure of ferrite phase.

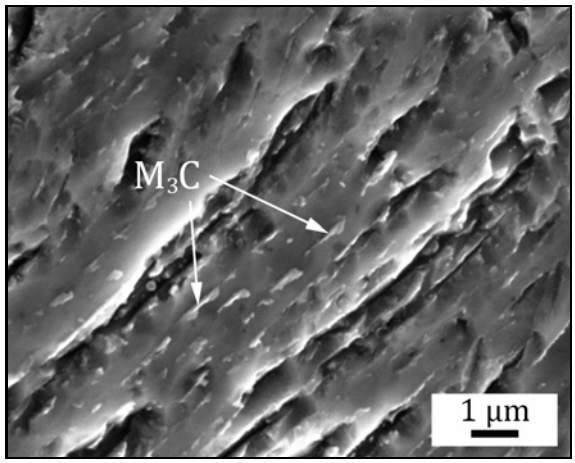

Fig. 7. Upper bainite in FZ of the weld, SEM (M_3C – carbide precipitates).

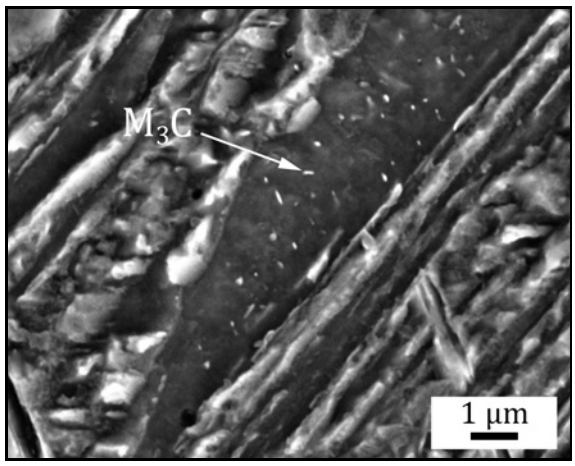

Fig. 8. Lower bainite in FZ of the weld, SEM (M_3C – carbide precipitates).

The upper and lower bainite can be distinguished in micrographs in Figs. 7 to 9. Upper bainite in Fig. 7 has laths of ferrite with coarse M_3C carbides precipitated at lath boundaries. However, carbides are finer and precipitate inside the laths in lower bainite as can be seen in SEM micrograph in Fig. 8 and in TEM micrographs in Fig. 9. The dark image in Fig. 9b reflects bright M_3C carbides in this image. Both ferrite (white motif) and M_3C carbide (dark motif) phases were identified in the electron diffraction pattern in Fig. 9c. The presence of these phases and their morphology confirms the presence of lower bainite. As the lower bainite is created at a lower temperature compared to upper bainite, the diffusion of carbon is lower, and carbides are finer in lower bainite in Fig. 8 than in upper bainite in Fig. 7.

Only a few small areas of martensite were found

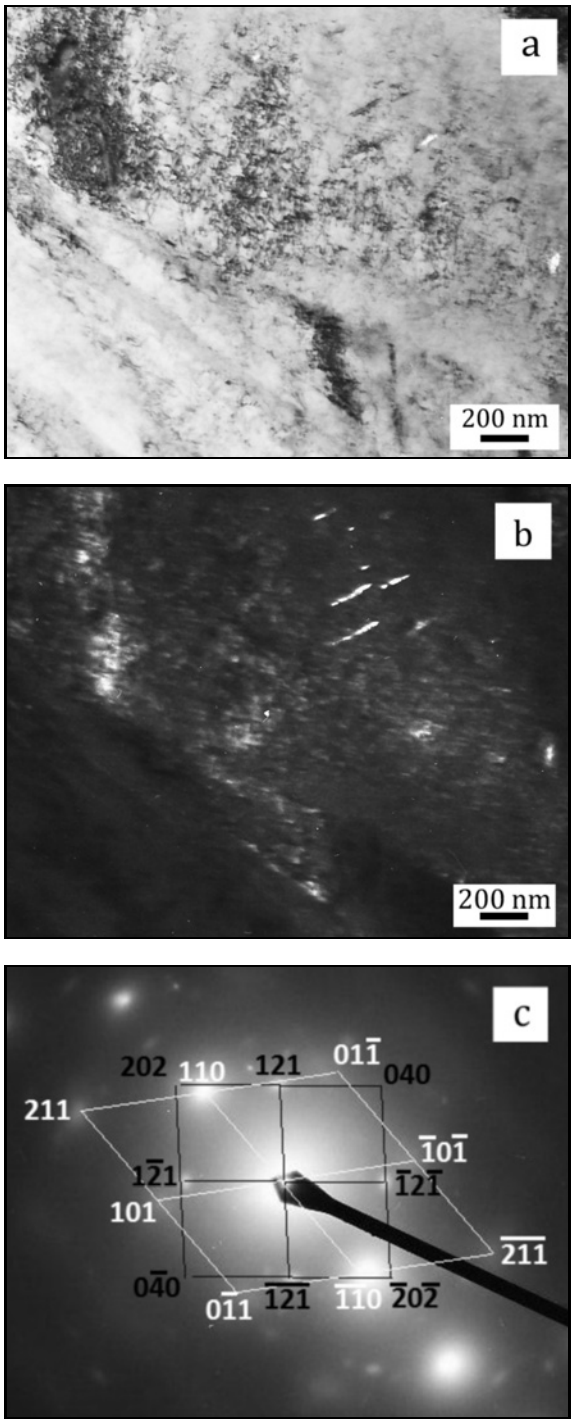

Fig. 9. Lower bainite in FZ of the weld: a) bright field TEM image, b) dark field TEM image with reflections of M_3C carbides, c) electron diffraction pattern (white motif – ferrite matrix, black motif – M_3C carbides).

in sub-structure of the FZ. These were identified by SEM in Fig. 10 and by TEM in Fig. 11. Morphological characteristics of low carbon martensite with retained austenite can be seen in Fig. 10. The martensite lath packets with the angle of 60° contain interlath re-

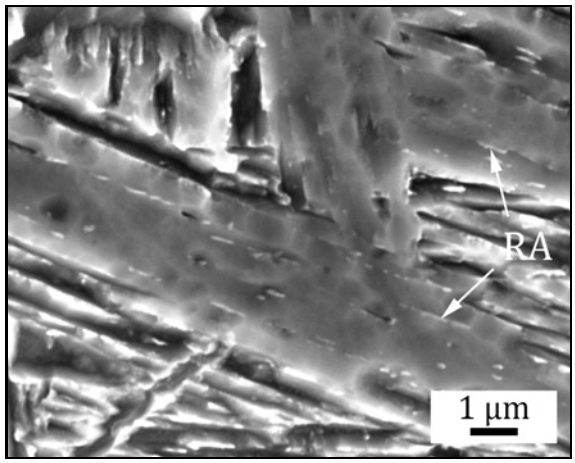

Fig. 10. Martensite with retained austenite in FZ of the weld, SEM (RA – retained austenite).

tained austenite (RA). Interlath retained austenite is also seen between the particular martensitic laths in Figs. 11a,b. The identification of martensite was confirmed by dark field image in Fig. 11b with reflections corresponding to the retained austenite (white areas). Since the martensite is a supersaturated solid solution of carbon in alpha ferrite, two phases can be identified in the electron diffraction pattern of martensite in Fig. 11c. Ferrite matrix represents the black motif and retained austenite represents the white motif in the electron diffraction pattern of martensite.

The microstructures within both HAZs in Figs. 12 and 13 were created by the effect of weld thermal cycle. As the chemical compositions of both steels are different, the different microstructures in both HAZs were observed. Since the DP600 steel contains a larger amount of alloying elements compared to BH220 steel, the HAZ microstructure near DP600 steel consisted mainly of lath microconstituents built in packets. The microstructures of HAZ were finer with the distance from the fusion boundary. The microstructure in the coarse-grained region of HAZ near DP600 steel in the vicinity of fusion boundary is documented in Fig. 12. Large prior-austenite grain size and all microconstituents typical for laser welded joints except martensite can be seen in Fig. 12. Proeutectoid ferrite (PF) and large areas of acicular ferrite (AF) can be seen at prior austenite grain boundary. Small areas of upper bainite (UB) and lower bainite (LB) are visible, too. The microconstituents created within the HAZ near DP600 steel were similar to those within the FZ, and therefore they were not documented in such details as it was in the case of the FZ. The HAZ microstructure near BH220 steel consists mainly of coarse ferrite and acicular ferrite as can be seen in Fig. 13. This is the consequence of lower content of carbon and alloying elements in BH steel compared to the DP steel.

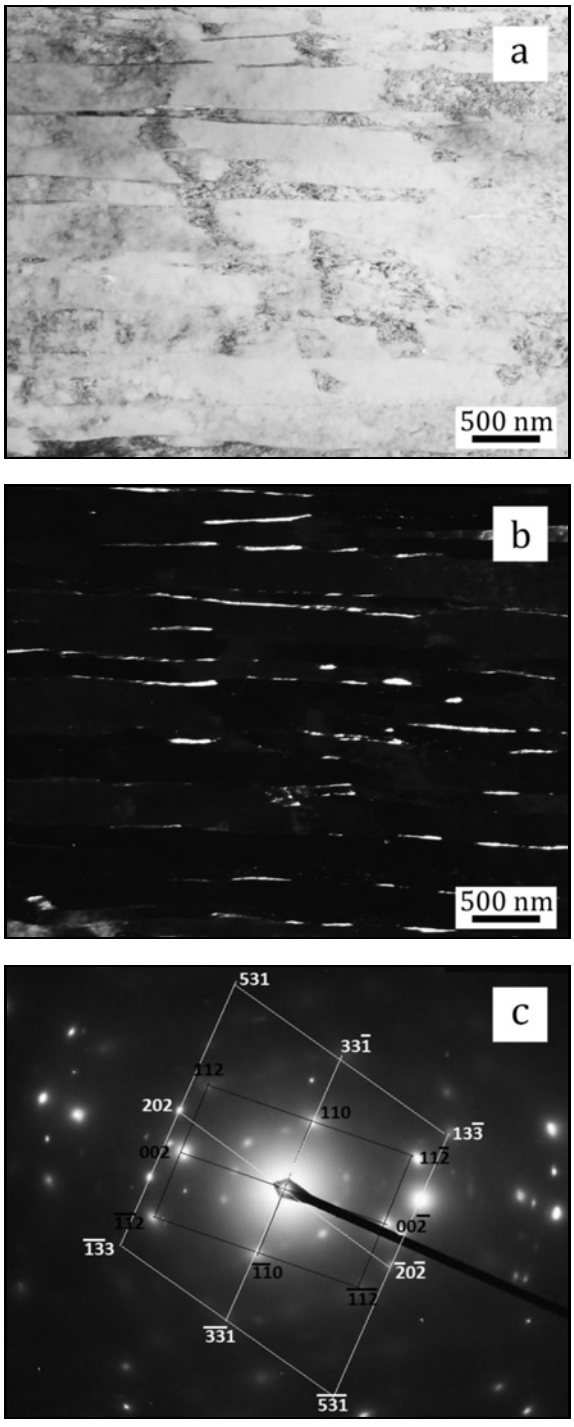

Fig. 11. Martensite with retained austenite in FZ of the weld: a) bright field TEM image, b) dark field TEM image with reflections of retained austenite, c) electron diffraction pattern (black motif – ferrite matrix, white motif – retained austenite).

3.4. Microhardness profile across the welded joint

The variation in microhardness profile across the FZ, HAZs, and BMs measured across the mid-section of the welded joint is presented in Fig. 14. The microhardness profile is characterized by an unsymmetrical shape, and with increased microhardness values in both HAZs from BMs towards the FZ. HAZ softening is visible in the vicinity of DP600 steel BM and marked by the circle. The hardness of DP600 steel BM was in the interval from 208 to 229 $HV_{0.1}$ and with an average value of 219 $HV_{0.1}$, and this value represents a ferritic-martensitic microstructure of DP600 steel. However, the microhardness in the interval from 85 to 135 $HV_{0.1}$ and with an average value of 110 $HV_{0.1}$ measured for BH220 steel represents a ferritic structure of the BH220 steel. The microhardness values in FZ were in the interval from 265 to 375 $HV_{0.1}$. The microhardness values within the FZ could be compared with works [29–31] that were devoted to laser welding

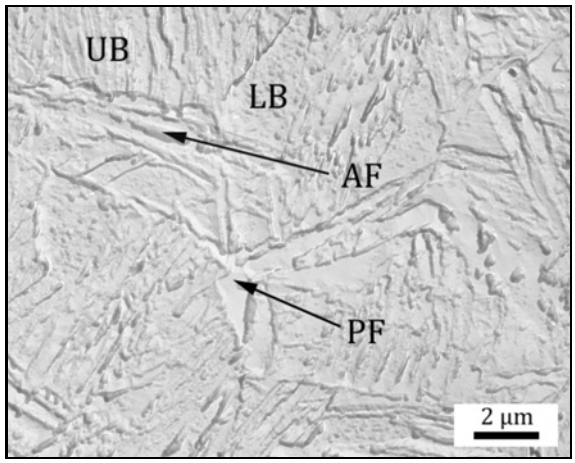

Fig. 12. The microstructures of HAZ near the DP600 steel, TEM (PF – pro-eutectoid ferrite at prior austenite grain boundary, AF – acicular ferrite, UB – upper bainite, LB – lower bainite).

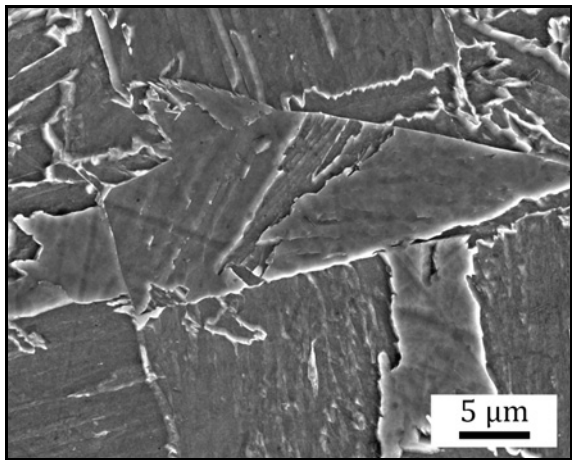

Fig. 13. The microstructures of HAZ near the BH220 steel, SEM.

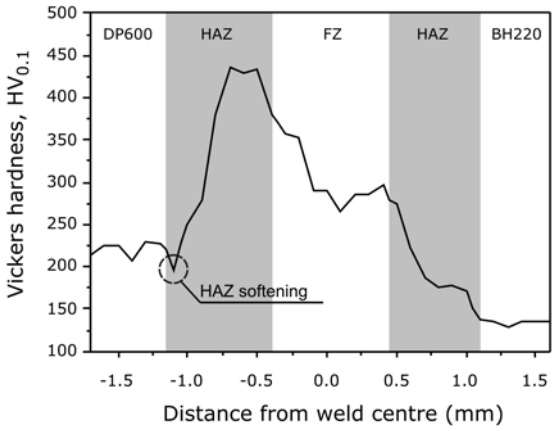

Fig. 14. Microhardness profile across the welded joint.

of DP600 steels. The FZ in these works reached hardness in the interval from 270 to 340 HV [29], from 310 to 360 HV [30], and from 300 to 370 HV [31]. The microhardness in HAZ near BH220 was in the interval from 135 to 298 $HV_{0.1}$ and the microhardness in HAZ near DP600 steel was from 195 to 435 $HV_{0.1}$. The value of 435 $HV_{0.1}$ was the highest measured microhardness, and it was measured in the coarse-grained region of HAZ. The smallest value in this HAZ was 195 $HV_{0.1}$ and was measured in the vicinity of DP600 steel BM and represents the softening region. This reduction of hardness in the tempered region of HAZ is minimal and in good agreement with works [29–31]. Authors of these works measured the minimal hardness about 190 HV [29, 30], or 200 HV [31]. The microhardness values confirm the identification of microstructural constituents.

3.5. Tensile properties of welded joint

The tensile tests showed the average joint strength of 340 MPa and an apparent average elongation of 8.9 %. The strength of welded joint reached the tensile strength of weaker BH220 steel, and it was in line with the microhardness results.

The elongation was less than the average value of both DP600 and BH220 steel. The lower elongation of welded joint compared to both BMs can be explained by strengthening of the weld by the welding process and minimal yielding of weld region, which was confirmed by microhardness profile across the welded joint (Fig. 14).

4. Discussion

4.1. Microstructure characteristics

The development of microstructure within the different sub-zones of a welded joint depends on the local thermal cycles characterized by the peak temperature and cooling rate reached during the welding process. By comparing peak temperatures with theoretical transformation temperatures in the time temperature transformation diagrams of welded steel, the evolution of microstructure can be described. This comparison is important mainly for DP steel because less variation in microstructure was observed in BH steel. The A_{c3} temperature which corresponds to the complete transformation to austenite for DP600 steel is according to work [28] about 900 ℃. The A_{c1} temperature which corresponds to the temperature at which the BM begins to transform to austenite is about 700 ℃. Both temperatures decrease due to the larger cooling rates during the laser welding process [28].

The microstructures within the FZ are the results of solidification behaviour and subsequent solid phase transformations, which are controlled by composition and cooling rate given by heat input. In this fast solidification process a large number of large austenite grains formed, which were columnar and orientated parallel to the direction of heat removing. Under the very fast cooling conditions following welding, these large prior austenite grains transformed to acicular ferrite, upper and lower bainite or martensite. The large prior austenite grain boundaries and acicular ferrite in the FZ can be seen in Fig. 4. The upper and lower bainite were identified according to the presence of M_3C carbide precipitates. In upper bainite in Fig. 7 coarse carbides precipitated at lath boundaries. Fine carbides inside the laths were observed in lower bainite in Figs. 8 and 9. Only small areas of laths of low-carbon martensite were found, and these were identified according to martensite lath packets with interlath retained austenite. These are visible in Figs. 10 and 11.

In the HAZ near DP600 steel and in the vicinity of the fusion boundary is coarse-grained region. In this region the peak temperature rises above A_{c3} (900 ℃) but is lower than the solid temperature which is the consequence of complete re-austenitization and rapid grain growth. During rapid cooling following welding, various microconstituents form. Acicular ferrite, pro-eutectoid ferrite, upper bainite, and lower bainite within this HAZ are documented in Fig. 12. As the peak temperatures decrease with the distance from the fusion boundary, austenitization is not complete; grains are finer, and less microstructure transformation occurs. Therefore, the only microstructure in the coarse-grained region of HAZ near DP600 steel was presented in the paper. In consequence of lower carbon and alloying elements content the microstructures in the coarse-grained region of HAZ near BH200 steel are composed of only coarse ferrite and acicular ferrite as can be seen in Fig. 13.

4.2. Microhardness profile across the welded joint

The microhardness across the welded joint varies significantly because of the phase transformations occurred in the FZ and HAZs during the welding thermal cycle. The fast heating and cooling rates associated with fibre laser welding result in the generation of acicular ferrite, upper and lower bainite, and martensite in the FZ and HAZ near DP600 steel. Harder microconstituents as upper and lower bainite and martensite created small areas within the larger areas of acicular ferrite but had the major contribution to the hardness increase and consequently increased the strength of the weld. This results in the maximal microhardness in the FZ of 375 $HV_{0.1}$, and the microhardness in HAZ near DP600 steel reaching a value of 435 $HV_{0.1}$, when compared with the microhardness of the BMs (219 $HV_{0.1}$ for DP600 steel and 135 $HV_{0.1}$ for BH220 steel). The reduction of microhardness in HAZ near DP600 steel to the value of 190 $HV_{0.1}$ represents the HAZ softening region in the vicinity of DP600 steel BM. The maximal microhardness in HAZ near BH steel was 298 $HV_{0.1}$, which indicates that some upper bainite could be present together with acicular ferrite in this area, but only ferrite and acicular ferrite were observed in HAZ near 220BH steel. The creation of harder microconstituents in welded joint is accompanied by the strength increase in the weld. The strengths of FZ and both HAZs were higher than that of BH220 steel BM and fibre laser welded tensile test specimens failed in the BH220 steel BM.

5. Conclusions

The fibre laser welding of dual phase DP600 steel with bake hardening 220BH steel was studied with a concentration on microstructure and its correlation with microhardness. The welds prepared with a fibre laser process were free of porosity or cracks, and their geometry was characterized by the slight concavity of the face and root sagging. These imperfections did not have the negative effect on the tensile strength of the joints.

Large areas of acicular ferrite were found in the FZ of the welded joint. The smaller areas were created by the lath microconstituents. Laths of upper and lower bainite and martensite were built in packets within a large columnar grain structure and were the consequence of rapid cooling. The microstructure of HAZ near DP600 steel consisted of acicular ferrite, upper and lower bainite, and martensite. Coarse ferrite and acicular ferrite were observed in HAZ near BH220 steel.

Microhardness profile across the welded joint was characterized by an unsymmetrical shape, with increased microhardness values in FZ, both HAZs, and with HAZ softening in HAZ near DP600 steel. The maximum microhardness across the welded joint was measured within the HAZ near DP600 steel with the value of 435 $HV_{0.1}$. The maximal hardness in the HAZ near BH220 steel reached 298 $HV_{0.1}$. The hardness in the FZ was in the interval from 265 to 375 $HV_{0.1}$. The tensile strength of the fibre laser welded joints reached the strength of the BH220 steel with all welded specimens failing in the BH220 steel.

Acknowledgement

This work was supported by the Slovak Research and Development Agency under the contract No. APVV-0281--12.

References

[1] Cui, Q. L., Parkes, D., Westerbaan, D., Nayak, S. S., Zhou, Y., Liu, D., Goodwin, F., Bhole, S., Chen, D. L.: Materials & Design, *90*, 2016, p. 516. doi:10.1016/j.matdes.2015.10.098

[2] Yan, D., Tasan, C. C., Raabe, D.: Acta Materialia, *96*, 2015, p. 399. doi:10.1016/j.actamat.2015.05.038

[3] Bandyopandyay, K., Panda, S. K., Saha, D. C., Baltazar-Hernandez, V. H., Zhou, Y. N.: Materials Science & Engineering A, *652*, 2016, p. 250. doi:10.1016/j.msea.2015.11.091

[4] Xu, W., Westerbaan, D., Nayak, S. S., Chen, D. L., Goodwin, F., Zhou, Y.: Materials & Design, *43*, 2013, p. 373. doi:10.1016/j.matdes.2012.07.017

[5] Fereiduni, E., Ghasemi Banadkouki, S. S.: Journal of Alloys and Compounds, *557*, 2013, p. 351. doi:10.1016/j.jallcom.2013.05.209

[6] Viňáš, J., Ábel, M.: Materials Science Forum, *818*, 2015, p. 239. doi:10.4028/www.scientific.net/MSF.818.239

[7] Wang, J., Yang, L., Sun, M., Liu, T., Li, H.: Materials & Design, *90*, 2016, p. 642. doi:10.1016/j.matdes.2015.11.006

[8] Broggiato, G. B., Cortese, L., Nalli, F., Russo Spena, P.: Procedia Engineering, *109*, 2015, p. 356. doi:10.1016/j.proeng.2015.06.243

[9] Schemmann, L., Zaefferer, S., Raabe, D., Friedel, F., Mattissen, D.: Acta Materialia, *95*, 2015, p. 386. doi:10.1016/j.actamat.2015.05.005

[10] Rossini, M., Russo Spena, P., Cortese, L., Matteis, P., Firrao, D.: Materials Science & Engineering A, *628*, 2015, p. 288. doi:10.1016/j. msea.2015.01.037

[11] Farabi, N., Chen, D. L., Zhou, Y.: Journal of Alloys and Compounds, *509*, 2011, p. 982. doi:10.1016/j.jallcom.2010.08.158

[12] Mazaheri, Y., Kermanpur, A., Najafizadeh, A.: Materials Science & Engineering A, *639*, 2015, p. 8. doi:10.1016/j.msea.2015.04.098

[13] Parkes, D., Westerbaan, D., Nayak, S. S., Zhou, Y., Goodwin, F., Bhole, S., Chen, D. L.: Materials & Design, *56*, 2014, p. 193. doi:10.1016/j.matdes.2013.10.087

[14] Parkes, D., Xu, W., Westerbaan, D., Nayak, S. S., Zhou, Y., Goodwin, F., Bhole, S., Chen, D. L.: Materials & Design, *51*, 2013, p. 665. doi:10.1016/j.matdes.2013.04.076
[15] Saha, D. C., Westerbaan, D., Nayak, S. S., Biro, E., Gerlich, A. P., Zhou, Y.: Materials Science & Engineering A, *607*, 2014, p. 445. doi:10.1016/j.msea.2014.14.034
[16] Sinha, A. K., Kim, D. Y., Ceglarek, D.: Optics and Laser in Engineering, *51*, 2013, p. 1143. doi:10.1016/j.optlaseng.2013.04.012
[17] Wu, Q., Gong, J., Chen, G., Xu, L.: Optics Laser Technology, *40*, 2008, p. 420. doi:10.1016/j.optlastec.2007.06.004
[18] Gong, H., Wang, S., Knysh, P., Korkolis, Y. P.: Materials & Design, *90*, 2016, p. 1115. doi:10.1016/j.matdes.2015.11.057
[19] Merklein, M., Johannes, M., Lechner, M., Kuppert, A.: Journal of Materials Processing Technology, *214*, 2014, p. 151. doi:10.1016/j.jmatprotec.2013.08.015
[20] Mei, L., Chen, G., Jin, X., Zhang, Y., Wu, Q.: Optics Laser Technology, *47*, 2009, p. 1117. doi:10.1016/j.optlaseng.2009.06.016
[21] Guo, W., Crowther, D., Francis, J. A., Thompson, A., Liu, Z., Li, L.: Materials & Design, *85*, 2015, p. 534. doi:10.1016/j.matdes.2015.07.037
[22] Meško, J., Zrak, A., Mulczyk, K., Tofil, S.: Manufacturing Technology, *14*, 2014, p. 355.
[23] Xu, F., Sun, G., Li, G., Li, Q.: Journal of Materials Processing Technology, *214*, 2014, p. 925. doi:10.1016/j. jmatprotec.2013.11.018
[24] Ma, J., Kong, F., Liu, W., Carlson, B. Kovacevic, R.: Journal of Materials Processing Technology, *214*, 2014, p. 1696. doi:10.1016/j.jmatprotec.2014.03.018
[25] Hazratinezhad, H., Mostafa Arab, N. B., Sufizadeh, A. R., Torkomany, M. J.: Materials & Design, *33*, 2012, p. 83. doi:10.1016/j.matdes.2011.06.070
[26] Lee, J. H., Park, S. H., Kwon, H. S., Kim, G. S., Lee, C. S.: Materials & Design, *64*, 2014, p. 559. doi:10.1016/j.matdes.2014.07.065
[27] Sharma, R. S., Molian, P.: Journal of Materials Processing Technology, *211*, 2011, p. 1888. doi:10.1016/j. jmatprotec.2011.06.009
[28] Krajewski, S., Nowacki, J.: Archives of Civil and Mechanical Engineering, *14*, 2014, p. 278. doi:10.1016/j.acme.2013.10.002
[29] Dong, D., Liu, Y., Yang, Y., Li, J., Ma, M., Jing, T.: Materials Science & Engineering A, *594*, 2014, p. 17, doi:10.1016/j.msea.2013.11.047
[30] Farabi, N., Chen, D. L., Li, J., Zhou, Y., Dong, S. J.: Materials Science & Engineering A, *527*, 2010, p. 1215. doi:10.1016/j.msea.2009.09.051
[31] Li, J., Nayak, S. S., Biro, E., Panda, S. K., Goodwin, F., Zhou, Y.: Materials & Design, *52*, 2013, p. 757. doi:10.1016/j.matdes.2013.06.021